Packing Density and Structural Heterogeneity of Insulin Amyloid Fibrils Measured by AFM Nanoindentation

Senli Guo and Boris B. Akhremitchev*

Department of Chemistry, Duke University, Durham, North Carolina 27708

Received January 23, 2006; Revised Manuscript Received March 13, 2006

A nanoindentation approach based on atomic force microscopy was applied to test the elastic properties of insulin amyloid fibrils. Fibrils exhibited a nearly elastic response to the compressive load. The results, corrected for the finite sample thickness effect, reveal that the fibril Young's modulus is considerably lower than the modulus of protein crystals, suggesting lower packing density in amyloid fibrils. Variation in elasticity among and within fibrils has been studied, showing that the Young's moduli of insulin fibrils have a relatively wide distribution of values, ranging from 5 to 50 MPa. Amyloid fibrils with higher modulus were found to be more wear-resistant during AFM scanning. The measured distribution of elasticity values of different fibrils together with wear-resistance tests indicates structural heterogeneity among fibrils, whereas the structure of individual fibrils appears to be homogeneous. The relative simplicity of the method used in this study can facilitate rapid collection of quantitative information related to the packing density and heterogeneity of fibrils formed by different proteins.

Introduction

More than 20 neurogenerative diseases have been associated with amyloid aggregation.[1] The ability to form amyloid structures is considered a generic property of polypeptide chains.[2] The propensity to form amyloid fibrils and the detailed organization within fibril structures depend on the specific amino acid sequence.[3] Over the past three decades, considerable attention has been focused on the aggregation mechanism and structures of amyloid fibrils.[1−7] It is widely accepted that amyloid fibrils of different proteins have a common cross β structure with β-strands oriented perpendicularly to the axis of the fibril.[3,5,6] Amyloid fibrils are relatively stable even in adverse chemical environments. For example, they are highly protease resistant.[8] Despite their stability, it appears that the packing of protein molecules within amyloid fibrils is not as dense as within globular proteins, as revealed by cryo-electron microscopy studies of the SH3 amyloid fibril structure.[9] This observation is supported by recent calorimetric measurements which indicate that amyloid fibrils have looser internal packing in comparison with globular proteins in the native folded state.[10] Information about the packing density of proteins inside fibrils remains scarce. Packing density has been related to the flexibility of protein molecules,[11] and thus the compactness of the amyloid fibril structure can be inferred by testing the elastic properties of fibrils. In addition, because nontoxic protein fibrils could be promising nanobiomaterials,[12−14] obtaining their mechanical properties at a high resolution is useful to the development of novel materials.

Atomic force microscopy (AFM) has been employed to reveal the structural features of amyloid fibrils.[15−18] In addition to mapping the topography of samples, AFM is often used in a force−scan modality. The force measurement modality employed in this study permits characterization of the mechanical properties of fibrils. This mechanical characterization of soft materials requires the simultaneous measurement of applied forces ranging from 10^{-11} to 10^{-8} N and the registration of the sample's resulting deformation with subnanometer accuracy. These values are extracted from the force-displacement curves collected during nanoindentation experiments employed here.

The AFM nanoindentation technique has been commonly used for quantitative measurements of local elasticity with high (~10 nm) spatial resolution,[19−27] including measurements of elastic properties of individual dendritic molecules[24] and individual nanofibers.[27] In these applications, the AFM tip is used as a nano-indenter. A small, measurable indentation results from the application of a suitable force to the AFM tip. The measured force-indentation dependences are processed to estimate the Young's modulus (also known as the elastic modulus) of the sample. The Young's modulus is obtained by applying appropriate mechanical models [28−30] to fit the indentation data. One of the major assumptions in applying these models is that the sample is treated as a semi-infinite homogeneous elastic solid.[22,23] However, when a tip indents a thin soft sample placed on a hard substrate, the indentation is affected by the underlying substrate if the radius of contact area is comparable to the sample thickness.[31] Since the thickness of fibrils (in the experiments reported here ranging from several nanometers to approximately 10 nm) is comparable with the tip radii (~10 nm and more), a correction due to the finite thickness of the sample is required for more accurate estimation of their Young's moduli.[22,23,25]

In this report, we apply the AFM nanoindentation technique for the direct characterization of internal packing in insulin fibrils. Amyloid aggregation has been associated with insulin production, storage, and delivery.[32] Insulin is known to readily form amyloid fibrils upon destabilization of the native state.[33] In particular, insulin fibrillates rapidly in acidic solutions with pH between 1 and 3.[33] Common morphological features observed during fibrillogenesis of insulin and other proteins, including α-synuclein and the B1 domain of protein G, have been used to suggest a general hierarchical mechanism of amyloid assembly.[34] This mechanism implies structural similarity of the resulting assemblies. However, a recent report on the amyloid aggregation of β2-microglobulin indicates that there are distinct competitive pathways in amyloid assembly.[7] In the present study, direct mechanical testing with AFM is employed

* To whom correspondence should be addressed. E-mail: Boris.a@duke.edu.

10.1021/bm0600724 CCC: $33.50
Published on Web 04/18/2006

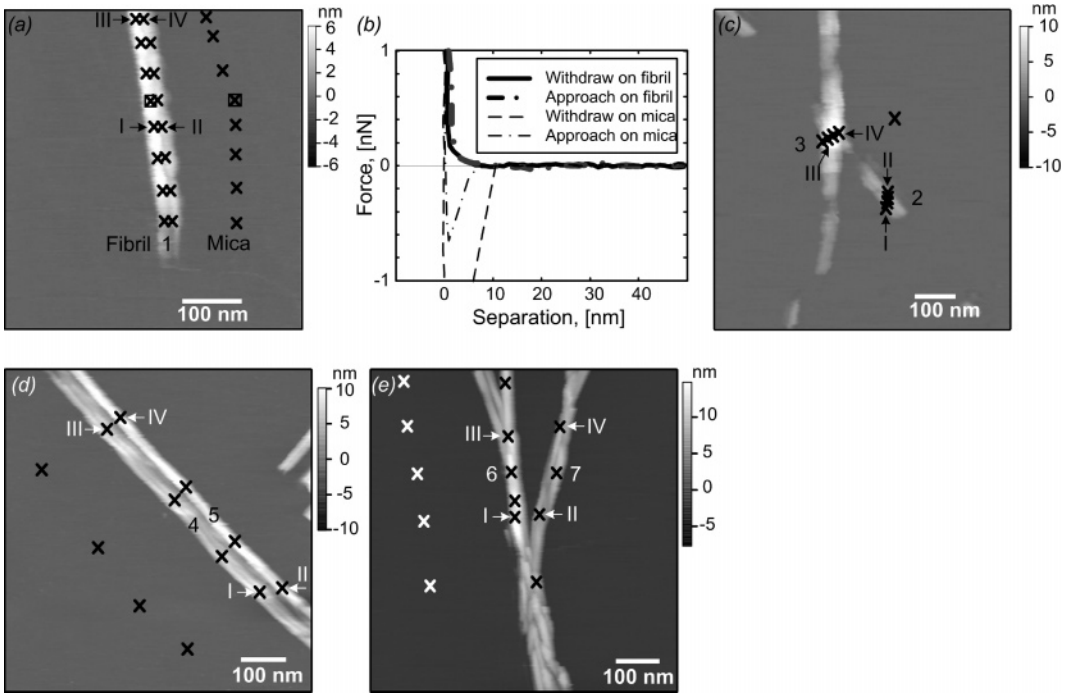

Figure 1. Height images (panels a, c, d, and e) of seven insulin fibrils (labeled by 1−7) that were used in nanoindentation experiments. The crosses on the images show the positions at which the force-displacement measurements were performed. The arrows indicate the positions at which the force plots shown in Figure 3 were collected. The substrate is a flat mica surface. Data collected on the substrate were used to calibrate the deflection sensitivity of the instrument. Panel b shows representative force-separation curves collected on the fibril and on the mica substrate at positions indicated with squares in panel a. The force curve on the fibril shows no adhesion and prominent indentation, whereas the force curve on the mica substrate shows large adhesion as well as large (∼5 nm) tip−surface distance where the instability in the tip position occurs during the probe approach.

to examine the heterogeneity in packing density between and within insulin fibrils. This testing involves nanoindentation of fibrils with the AFM probe that provides the effective elastic modulus of fibrils. Similarity between modulus values that are obtained on individual fibrils indicates the validity of the nanoindentation approach in amyloid fibril characterization. A similar nanoindentation approach has been used to characterize the elasticity of poly(L-lactic acid) nanofibers.[27]

The measured Young's moduli of insulin fibrils indicate that insulin fibrils possess looser internal packing compared with globular protein crystals. In addition, the statistical distribution of the finite-thickness corrected moduli shows that some filaments have a significantly higher elastic modulus indicating structural heterogeneity between simultaneously prepared fibrils. This observation is supported by higher wear resistance of fibrils with larger elastic moduli.

Materials and Methods

Sample Preparation. Bovine insulin solutions (5 mg/mL) were prepared by dissolving bovine insulin (Sigma-Aldrich, St. Louis MD; used as received) in a 10 mM HCl solution. Insulin solutions were incubated in polypropylene microcentrifuge tubes (Fisher Scientific, Pittsburgh, PA) at 80 °C for 48 h to prepare mature insulin fibrils.[33] After preparation, the fibril solutions were diluted with 10 mM HCl solution to the total concentration of 0.5 mg/mL and then centrifuged at 3000 rpm (MiniSpin Plus centrifuge, Eppendorf, Westbury, NY) for 30 s to separate soluble insulin species. The precipitates were collected and washed by adding the same volume of 10 mM HCl as the volume of removed liquid. Fibrils were washed by gentle shaking of the centrifuge tube. This separation procedure was repeated twice more. Fibril samples for AFM experiments were prepared by adding 25 μL of diluted fibril solution onto freshly cleaved mica substrate (grade V-1, SPI Inc., West Chester, PA). Fibrils were allowed to absorb onto the mica substrate for about 1 min. Excess fibrils were removed by rinsing the sample with 35 μL of 10 mM HCl solution five times.

AFM Measurements. All AFM measurements reported here (including force−displacement and topographic mapping) were performed using a Molecular Force Probe 3D AFM (MFP-3D, Asylum Research, Santa Barbara, CA). Silicon nitride probes (model NP-S20, Veeco, Santa Barbara, CA) with a nominal spring constant of 0.32 N/m were used in all measurements. Spring constants were measured using the thermal noise method.[35] The spring constants of the two batches of probes used in our experiments were 0.22 and 0.36 N/m.

AFM measurements were performed with samples immersed in 10 mM HCl solution. The assembled apparatus was allowed to equilibrate for approximately 2 h prior to each experiment to reduce thermal drift. After the equilibration, topographic images were collected using the AC imaging mode (also known as tapping mode) and the scan rate was kept 1 Hz. Fibrils were identified in the resulting maps, and typical shapes were selected for the indentation measurements. Several different positions along the selected fibril were chosen for performing indentation measurements, which involved the collection of a series of force curves. Each force curve consisted of a force-displacement record collected during reciprocating probe motion toward and away from the sample. The probe started motion toward the sample from the height of approximately 200 nm above the surface that continued until the predetermined deflection of the force-sensing cantilever was reached. Then the motion was reversed bringing the probe to approximately the initial height above the surface. Five force curves were collected at each fibril location as well as on the mica substrate close to the measurement point at the fibril (see Figure 1). Measurements on the substrate were used to calibrate the deflection sensitivity of the instrument that is necessary to convert force−displacement measurements into force vs tip−sample separation dependences. In all force-displacement measurements, indentation continued until a maximum level of compressive force corresponding to the cantilever deflection of 8 nm was reached. After completing force measurements, another

topographic image at the same position was collected to confirm that the sample's drift was small during the period of force measurements.

AFM Tip Radius Measurements. Manufacturer-provided tip radii of curvature of the silicon nitride probes range from 10 to 40 nm. The probes were imaged using a scanning electron microscope (SEM, Philips XL30) after performing AFM imaging and force measurements. The radius of the tip was determined by fitting a paraboloidal profile to the scanning electron micrograph of the tip. Due to the small tip radius and low density of silicon nitride this measurement procedure included approximately 10 nm uncertainty. A radius of 30 nm was used in the data analysis according to the SEM measurements. The tip radius uncertainty indicated above results in approximately 20% error in the calculated elastic modulus. This error is comparable to the error arising due to uncertainty in the spring constant (usually 20% error is quoted for the algorithm that was used to measure the spring constant).[36]

Data Analysis. Upon collection, force curves were exported as ASCII files and processed with a custom program written in Matlab (MathWorks, Inc., Natick, MA). The raw cantilever deflection vs probe displacement measurements have been converted into force−separation relations using the tip spring constants and the cantilever deflection sensitivities.[37] Deflection sensitivity values were extracted from the measurements of the reference points on the mica substrate. It is important to note that accuracy in measuring small indentation values is significantly affected by the accuracy of the deflection sensitivity calibration. Our measurements indicate that due to variation in the deflection sensitivity across the surface the error in elastic modulus can be as high as 50%, whereas the modulus error associated with the statistical error of measuring deflection sensitivity at the same location is close to 20% (data not shown). Therefore, measuring the deflection sensitivity at a position close to the location of indentation measurement provides a more accurate estimate of the elastic modulus.

In the analyses of the force−indentation data, the AFM tip apex is approximated as an axisymmetric paraboloidal probe to estimate the radius of curvature. Another analytical model that is commonly used to analyze force−indentation dependence is a conical tip model.[21] Given the value of typical indentation measured in this work (∼1 nm) and the much larger tip radius of curvature (∼30 nm), selection of this model would not be justified and would result in a large error in the estimated elastic modulus.[22]

According to the Hertzian model, the force-indentation relation is given by[31]

$$F = \frac{4ER^{1/2}}{3(1-\sigma^2)}\delta^{3/2} \quad (1)$$

Here F is the load, δ is the indentation, R is the probe's radius of curvature, E is the Young's modulus, and σ is the Poisson's ratio of the elastic solid. When using eq 1 to calculate the Young's modulus, it is essential to determine the tip−sample contact point between the probe and the surface that is necessary for an accurate calculation of the indentation, δ. It is noted that eq 1 can be rewritten in a way that avoids this limitation and allows calculation of the Young's modulus from the force vs tip−sample separation dependence without accurate measurements of the contact point. With some constant C, the estimated tip−sample separation Δ is related to the indentation as $\delta = C - \Delta$. Therefore, eq 1 can be written as

$$F^{2/3} = C^* - \left[\frac{4}{3}\frac{E\cdot R^{1/2}}{(1-\sigma^2)}\right]^{2/3}\cdot\Delta \quad (2)$$

where C^* is another constant that depends on the selection of the tip−sample contact point. In this form, the Young's modulus is calculated from the linear slope of the $F^{2/3}$ vs Δ dependence and using the known or estimated values of the tip radius and Poisson's ratio. A Poisson ratio value $\sigma = 0.3$ is taken as a reasonable guess for fibrils. This assumption might result in systematic error of ∼10%, which is smaller than the uncertainty in cantilever's spring constant.[36]

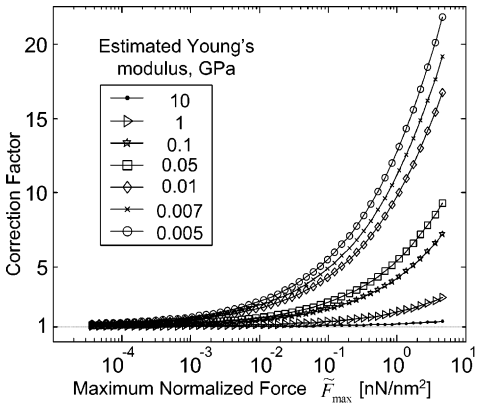

Figure 2. Correction factors for the finite sample thickness effect. The graphs show the dependence of the correction factors on the maximum normalized force. The correction factors were calculated for several samples with different Young's modulus. An apparent value of the Young's modulus for each line is indicated in the insert.

During data processing the goodness of the linear fit was estimated by calculating the r^2 values.[38] The data corresponding to r^2 values less than 0.5 were discarded. Discarded data amounted to less than 5% of the data used in the analysis. The mean r-square value for all linear regression analysis was 0.73.

Figure 1b shows typical force−separation curves collected on the fibril and on the mica substrate nearby at points indicated by the solid squares in Figure 1a. It can be noted that the approach−withdraw cycle on the mica is accompanied by a large adhesion, whereas no adhesion has been observed on the insulin fibril. The elastic restoration part of the force curves collected on the fibril during the unloading part of the approach−withdraw cycle was used for Young's modulus calculations. Only the deflection forces exceeding forces on the tip far from the surface (∼10 nm) by more than 70 pN were considered in modulus calculations as indicated in Figure 4 below.

It is expected that the indentation made by the AFM tip depends on the fibril thickness as a result of the substrate effect. Correction factors were calculated using an integral equation model that considers indentation of an infinitely wide elastic slab bonded to the elastic semispace by a paraboloidal axisymmetric tip.[39] At each measurement point, the correction factor depends on the maximum applied load, the sample's thickness, the Poisson's ratio, the Young's modulus, and the tip's radius of curvature. This multidimensional dependence can be condensed into fewer parameters with the introduction of normalized force.[22] Normalized forces are calculated according to the following equation:[40]

$$\tilde{F} = F\cdot R(1-\sigma^2)/h^3 \quad (3)$$

with this the correction factors depend only on two parameters: the maximum normalized force and the uncorrected Young's modulus values. The maximum normalized forces are calculated using the maximum values of the compressive forces applied to the samples during Young's modulus measurements. The uncorrected Young's modulus is estimated according to eq 2. Figure 2 shows dependencies of the correction factors on the maximum normalized forces for several values of uncorrected Young's modulus when the top layer is much softer than the substrate.[22] The Supporting Information contains a more detailed description of the correction factor calculation procedure.

Results and Discussion

Morphologies and Height Distributions. Force−indentation data were collected on seven insulin fibrils prepared under identical conditions. Figure 1a, c, d, and e shows morphologies

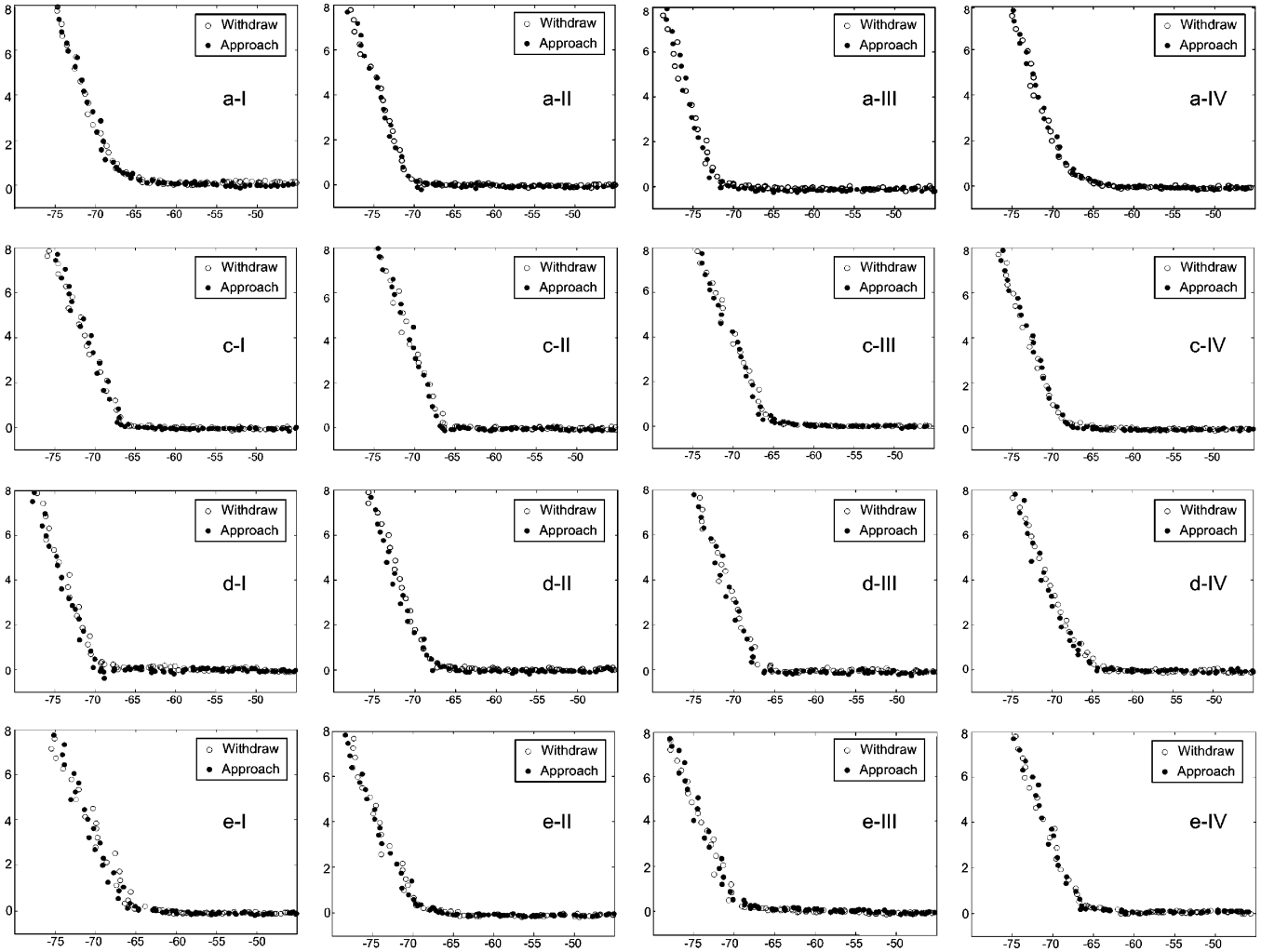

Figure 3. Cantilever deflection vs probe displacement curves including approach and withdraw curves collected at the positions indicated by the arrows in Figure 1. The unit of both axes is nanometer.

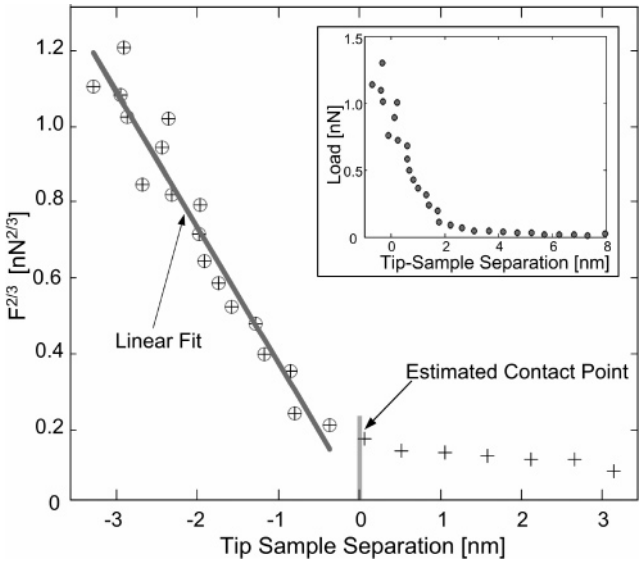

Figure 4. Typical force−indentation plot at the fibril. Here, the ordinate axis is the force in the power of 2/3 and the abscissa axis is the tip−sample separation. Linear fit to the data is indicated by the solid line. Force values that are used in the linear fit are indicated by circles around crosses. Slope of this line is used to extract an apparent Young's modulus using eq 2 in the text.

of seven fibrils (labeled with numerals from 1 to 7) in four samples with the positions at which the force plots have been collected (labeled with crosses in the images). Based on the tip position, the height of the fibrils at each measurement point has been determined from the topographic images. Examined fibrils exhibited variable morphological features such as twisted ribbonlike structures, parallel tubules, and rod bundles also observed by others.[18] A broad height distribution has been detected, ranging from 2.5 to 14 nm. However, no particles of prefibrillar aggregates were found around fibrils.[18] A larger scale image that confirms this observation is included in the Supporting Information. This is attributed to the aspects of the sample preparation procedure that involved separation of components by centrifugation.

Young's Moduli of Insulin Fibrils. Figure 1b shows representative force plots on the mica and on the insulin fibril, respectively. The force plots on the fibril display no adhesion compared with the force plots on the substrate. Absence of adhesion in the indentation experiments facilitates application of a simple Hertz model to estimate the elastic modulus of fibrils (because no adhesion is considered in this model). In addition, the force plots show no significant indentation hysteresis during the approach−withdraw cycle, which points to almost purely elastic response of the fibril to the compressive load. Figure 3 shows the approach−withdraw force plots collected on the above seven fibrils at locations that are indicated by the arrows in Figure 1. These force plots were collected at different representative positions including: the overlapping location of two fibrils, the interface of intertwined protofilaments, as well

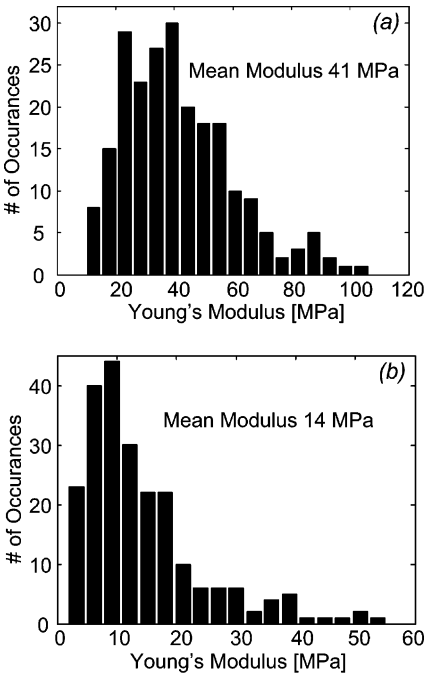

Figure 5. Apparent cumulative Young's modulus distribution (panel a) measured on all fibrils. Panel *b* shows the finite thickness-corrected modulus distribution.

as the thicker and thinner parts of twisted ribbonlike fibrils (similar to the ridge and the groove of the helical structure). Absence of indentation hysteresis also indicates that the AFM tip probably does not damage fibrils during indentation experiments and that the fibrils are in good contact with the substrate.

One typical result of the force−indentation measurement is shown in Figure 4. Here force in power of 2/3 (crosses) is plotted against the tip−sample separation together with the best linear fit (the solid line). The tip−sample separation values used in Figure 4 were adjusted to show the expected tip−sample contact point at zero separation. The short vertical line in the figure indicates this position. It can be noted that determination of the contact point by visual inspection of the original force−indentation dependence (shown in the insert in Figure 4) might be inaccurate due to small short-range repulsive forces experienced by the tip near the contact point. Force measurements that are used in the linear fit are indicated with circles around the data points. The slope of the fit line gives a Young's modulus of 27 MPa and an r^2 coefficient of 0.94. The obtained Young's modulus value is significantly lower than the Young's modulus of globular protein crystals, which usually range from 200 MPa to 1 GPa.[41,42] This observation can be further supported if the finite thickness correction is applied as will be discussed below.

Since fibrils are thin and soft, finite thickness effects have been considered during Young's modulus estimations. For the measurement shown in Figure 4, the correction factor was calculated to be 4.0, which decreases the value of Young's modulus to about 7 MPa. In other measurements reported here, the maximum of the correction factor ranges from 8.3 for the location on a fibril with a height of 2.5 nm and a maximum normalized force of 2.7 nN/nm^2 to the minimum value of 1.9 for the location on a fibril with a height of 13.7 nm and a maximum normalized force of 0.023 nN/nm^2. As displayed in Figure 5, panels a and b, before the correction the average Young's modulus is 41 MPa (average over all measured points on different fibrils), but after the correction was applied, the average value decreased to 14 MPa. Similar correction factors were obtained using the model of indentation of samples with

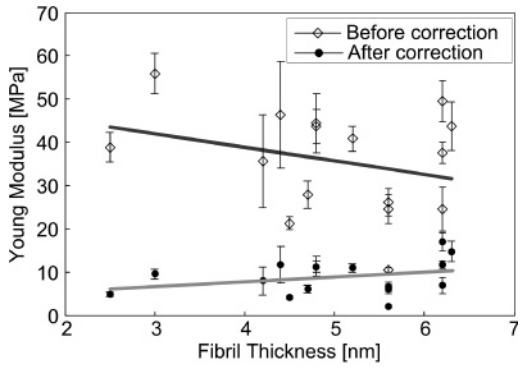

Figure 6. Young's moduli before and after the finite thickness correction for the fibril shown in Figure 1a. Solid lines included in the graph provide a guide to an eye.

finite thickness developed by Dimitriadis [23] (data not shown). Figure 6 shows that for the fibril shown in Figure 1a, the uncorrected Young's modulus values correlate inversely with the thickness of the fibril and that the finite thickness correction procedure removed this correlation. After the correction is performed, a small positive correlation can be noted. This correlation could be attributed to the limitations of the finite layer model or actually a property of the sample.

Another factor that might affect estimates of the elastic modulus reported here is the local geometry of the tip−sample contact. The upper limit for the influence of this geometrical factor can be estimated if instead of the tip radius the reduced radius is used in eq 2. The reduced radius r is calculated according to $1/r = 1/R_{tip} + 1/R_{fibril}$ where R_{tip} is the radius of curvature of the indenting tip and R_{fibril} is the radius of the fibril. The radius of the fibril can be estimated from the topographic images taking into account convolution of the fibril shape by the probe. When such an estimate is applied to the results shown in Figure 4, the reduced radius is $r = 20$ nm and the estimated Young's modulus becomes 33 MPa. This increase in the modulus is the upper limit for the Young's modulus because it assumes a spherical sample shape and neglects the finite thickness effects. With the finite thickness effects taken into account, the upper estimate of Young's modulus becomes 10 MPa, which is still considerably lower than the modulus for the crystalline proteins.[41]

For each of the seven fibrils labeled in Figure 1, the average Young's modulus results are listed in Table 1. The errors indicated in the table correspond to the measured standard deviation of the mean. The Young's modulus results presented in Table 1 show that the modulus of insulin amyloid fibrils is in the low tens of megapascals. A comparison of the relatively low values of the Young's modulus measured here with the modulus of protein crystals (200 MPa to 1 Gpa)[41] leads to the conclusion that the internal packing density in fibrils is not as high as in crystals of the native folded state. This observation is supported by the observed volume expansion of insulin molecules during amyloid formation[43] and also agrees with the suggestion of a loose internal structure of β2-microglobulin amyloid fibrils.[10] It has to be noted that the above conclusions about the insulin volume change and lower level of β2-microglobulin packing were based on calorimetric experimental techniques, whereas the results obtained here are based on a different and independent experimental approach. The loose structure of amyloid fibrils is further supported by the presence of a hollow core and partial unfolding of the native state in the structure of mature amyloid fibrils of the SH3 domain.[9] In addition, recent X-ray diffraction measurements of the fibrillar

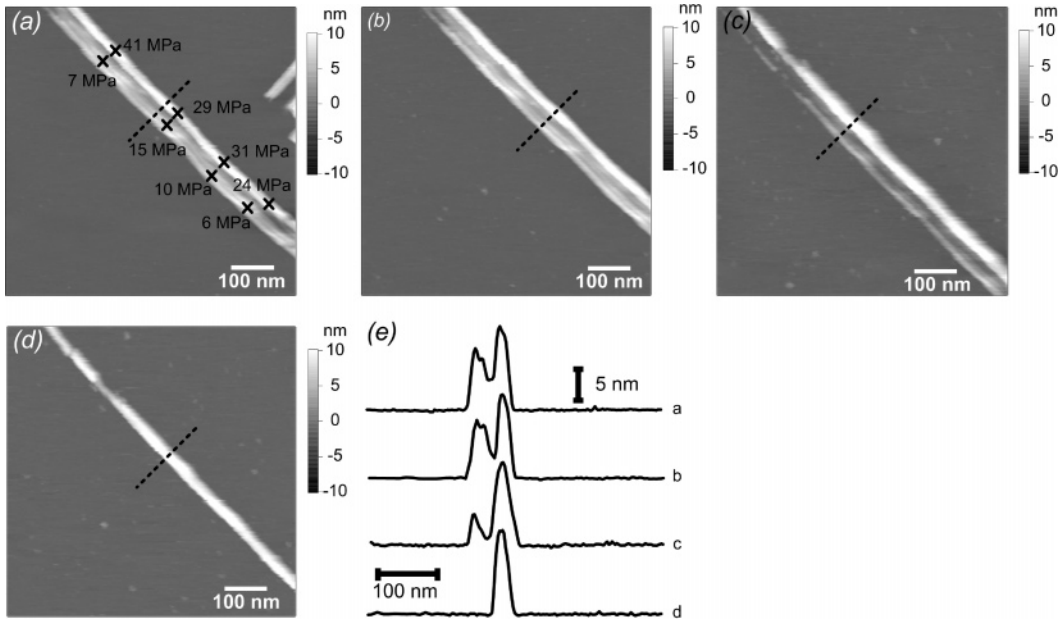

Figure 7. Sequential topographic images (panels a−d) of two fibrils and indicate the substantial material loss from the fibril with lower elasticity during the topography scanning. Young's modulus values are indicated next to the measurement points in panel a. The line plots in panel e show the cross sections of the topographic maps, and the position of these sections is indicated with a dashed line in the images. The fibril with higher elastic modulus shows much higher wear resistance.

Table 1. Young's Moduli of Seven Fibrils Indicated in Figure 1

fibril number	1	2	3	4	5	6	7
mean height (nm)	5.0 ± 1.1	4.0 ± 0.6	9.4 ± 1.6	7.1 ± 0.6	11 ± 2	12.1 ± 1.0	8.9 ± 0.8
uncorrected modulus (MPa)	36 ± 5	57 ± 5	54 ± 7	34 ± 3	64 ± 6	41 ± 6	35 ± 4
corrected modulus (MPa)	9 ± 2	12.6 ± 1.4	25 ± 4	9.6 ± 1.0	31 ± 4	19 ± 3	13 ± 3

structures from fragments of prion protein[3] indicate that individual protofilaments in fibrils are separated by water molecules, resulting in a lower packing density and possibly low elastic modulus of fibrils. It appears that a relative looseness of packing might represent a common property of amyloid fibrils.[9,44] Testing of this suggestion requires additional measurements of packing density of fibrils from different proteins and at different maturation stages.

It can be noted that for fibrils with relatively uniform thickness (all fibrils except Fibril 1) the standard deviation of the Young's modulus measured at each fibril is below 25% of the average value for corresponding fibrils, whereas the mean modulus value ranges from 10 to 30 MPa. The variation in the average values of the modulus shown in Table 1 appears to be statistically significant for some fibrils, whereas the values along the fibril vary much less significantly. In addition, the distribution of the modulus values measured for a single fibril might be affected by the precision of the probe positioning. The magnitude of modulus variation is also seen in the histogram of the Young's modulus values, plotted in Figure 5b. The graph shows that this distribution has a long tail reaching up to three times the mean modulus value. It was noted that the high modulus values are not associated with the failure to account for the finite thickness effect as illustrated below. Some of the high Young's modulus values that are seen in the tail of the distribution in Figure 5b were collected on one of the two fibrils shown in Figure 1d. These two parallel fibrils possess significantly different modulus values, as indicated in Figure 7a. In addition to having different moduli, these fibrils exhibit remarkably different wear resistance when scanned repeatedly with the AFM probe. The series of images shown in Figure 7a−d indicate that the fibril with a lower modulus is much less wear-resistant than the fibril with a higher modulus. The presence of two adjacent fibrils in the image might imply that the topographic maps were affected by the double tip artifact. We note that the double tip artifact can be excluded from consideration here because no double tip artifact is found on the single fibril visible on the right-hand side of Figure 7a, which possesses the same height as parts of fibril 5. In addition, careful examination of the height variation of the two parallel fibrils indicates that there is no synchronous height variation for these two fibrils (as shown in Figure 7a−c), indicating that fibril 4 is not an artifact. The line-plot panel of Figure 7e shows a sequence of the height cross-sections for the series of images indicating a dramatic material loss as a result of AFM scanning. The results of the wear resistance test are in agreement with the Young's modulus measurements; this agreement provides evidence to support the reliability of the Young's modulus measurements.

The observed variation in the Young's modulus indicates that fibrils produced under identical conditions and even neighboring regions of the sample might exhibit different mechanical properties that can be related to differences in internal packing environments among fibrils.[45] Different internal packing environments indicate structural heterogeneity among fibrils. It is possible that the observed packing heterogeneity results from the chemical heterogeneity due to deamidation of insulin molecules.[45] It can be noted that this structural heterogeneity is not unique to insulin amyloid fibrils. Structural differences were observed in amyloid aggregates of β2-microglobulin resulting from the competitive aggregation pathways that exist under different solution conditions.[7] Also, TEM and NMR studies of amyloid aggregates produced from β-amyloid(1−40) peptide under slightly different conditions indicate significant difference

in supramolecular structure.[46] The Young's modulus differences observed here indicate that even fibrils prepared under identical conditions and with similar morphology might exhibit variation in the internal packing density and therefore different supramolecular structure. Also low variation of modulus values along the fibrils indicates persistence of the same supramolecular structure along each fibril. This observation is in agreement with the observed inheritance of supramolecular structure for β-amyloid fibrils[46] suggesting that different assembly pathways are present simultaneously during insulin fibrillation.

Conclusions

AFM was applied for the mechanical testing of individual amyloid fibrils of insulin in order to quantify the Young's modulus of the fibrils. The reported approach includes an accurate measurement of indentation by calibration of the deflection sensitivity in the close proximity of the measurement point. Young's modulus values were extracted using a paraboloidal tip model. The effect of the finite sample thickness on the estimated modulus values was considered, and the correction factor approach was used to adjust the modulus values. The consistency of measured values was confirmed by the difference in the wear resistance of fibrils with different moduli.

Indentation measurements indicate that the Young's modulus of insulin amyloid fibrils ranges from several megapascals to a few tens of megapascals. These values were used to infer the lower packing density inside fibrils in comparison with globular proteins. In combination with the data available for amyloid fibrils produced from other proteins, this observation supports the suggestion that this lower packing might be a general feature of all amyloid fibrils.[9,44] The measured variation in elasticity together with different wear resistance indicates internal structural heterogeneity between the fibrils. Similar values of elasticity along the fibrils indicate that the same structure persists along the amyloid fibril.

Supporting Information Available. A detailed description of the correction factor calculation procedure. This material is available free of charge via the Internet at http://pubs.acs.org.

References and Notes

(1) Stefani, M.; Dobson, C. M. *J. Mol. Med.* **2003**, *81*, 678−699.
(2) Dobson, C. M. *Nature* **2003**, *426*, 884−890.
(3) Dobson, C. M. *Nature* **2005**, *435*, 747−749.
(4) Sipe, J. D.; Cohen, A. S. *J. Struct. Biol.* **2000**, *130*, 88−98.
(5) Jiménez, J. L.; Nettleton, E. J.; Bouchard, M.; Robinson, C. V.; Dobson, C. M.; Saibil, H. R. *Proc. Natl. Acad. Sci. U.S.A.* **2002**, *99*, 9196−9201.
(6) Nelson, R.; Sawaya, M. R.; Balbirnie, M.; Madsen, A. O.; Riekel, C.; Grothe, R.; Eisenberg, D. *Nature* **2005**, *435*, 773−778.
(7) Gosal, W. S.; Morten, I. J.; Hewitt, E. W.; Smith, D. A.; Thomson, N. H.; Radford, S. E. *J. Mol. Biol.* **2005**, *351*, 850−864.
(8) Zurdo, J.; Guijarro, J. I.; Dobson, C. M. *J. Am. Chem. Soc.* **2001**, *123*, 8141−8142.
(9) Jimenez, J. L.; Guijarro, J. I.; Orlova, E.; Zurdo, J.; Dobson, C. M.; Sunde, M.; Saibil, H. R. *EMBO J.* **1999**, *18*, 815−821.
(10) Kardos, J.; Yamamoto, K.; Hasegawa, K.; Naiki, H.; Goto, Y. *J. Biol. Chem.* **2004**, *279*, 55308−55314.
(11) Halle, B. *Proc. Natl. Acad. Sci. U.S.A.* **2002**, *99*, 1274−1279.
(12) MacPhee, C. E.; Dobson, C. M. *J. Am. Chem. Soc.* **2000**, *122*, 12707−12713.
(13) Hamada, D.; Yanagihara, I.; Tsumoto, K. *Trends Biotechnol.* **2004**, *22*, 93−97.
(14) MacPhee, C. E.; Woolfson, D. N. *Curr. Opin. Solid State Mater. Sci.* **2004**, *8*, 141−149.
(15) Xu, S.; Bevis, B.; Arnsdorf, M. F. *Biophys. J.* **2001**, *81*, 446−454.
(16) Zhu, M.; Souillac, P. O.; Ionescu-Zanetti, C.; Carter, S. A.; Fink, A. L. *J. Biol. Chem.* **2002**, *277*, 50914−50922.
(17) Kad, N. M.; Myers, S. L.; Smith, D. P.; Smith, D. A.; Radford, S. E.; Thomson, N. H. *J. Mol. Biol.* **2003**, *330*, 785−797.
(18) Jansen, R.; Dzwolak, W.; Winter, R. *Biophys. J.* **2005**, *88*, 1344−1353.
(19) Tao, N. J.; Lindsay, S. M.; Lees, S. *Biophys. J.* **1992**, *63*, 1165−1169.
(20) Domke, J.; Radmacher, M. *Langmuir* **1998**, *14*, 3320−3325.
(21) A-Hassan, E.; Heinz, W. F.; Antonik, M. D.; D'Costa, N. P.; Nageswaran, S.; Schoenenberger, C.; Hoh, J. H. *Biophys. J.* **1998**, *74*, 1564−1578.
(22) Akhremitchev, B. B.; Walker, G. C. *Langmuir* **1999**, *15*, 5630−5634.
(23) Dimitriadis, E. K.; Horkay, F.; Maresca, J.; Kachar, B.; Chadwick, R. S. *Biophys. J.* **2002**, *82*, 2798−2810.
(24) Shulha, H.; Zhai, X.; Tsukruk, V. *Macromolecules* **2003**, *36*, 2825−2831.
(25) Kovalev, A.; Shulha, H.; Lemieux, M.; Mykhkin, N.; Tsukruk, V. *J. Mater. Res.* **2004**, *19*, 716−728.
(26) Sun, Y.; Guo, S.; Walker, G. C.; Kavanagh, C. J.; Swain, G. W. *Biofouling* **2004**, *20*, 279−289.
(27) Tan, E. P. S.; Lim C. T. *Appl. Phys. Lett.* **2005**, *87*, 113106.
(28) Hertz, H. J. *Reine Angew. Math.* **1881**, *92*, 156−171.
(29) Boussinesq, J. *Applications des Potentiels a l'Etude de l'Equilibre et du Mouvement des Solides Elastiques*; Gauthier-Villars: Paris, 1885.
(30) Sneddon, I. N. *Int. J. Eng. Sci.* **1965**, *3*, 47−57.
(31) Johnson, K. L. *Contact mechanics*; Cambridge University Press: Cambridge, U.K., 1985.
(32) Wang, W. *Int. J. Pharm.* **2005**, *289*, 1−30.
(33) Brange, J.; Andersen, L.; Laursen, E. D.; Meyn, G.; Rasmussen, E. *J. Pharm. Sci.* **1997**, *86*, 517−525.
(34) Khurana, R.; Ionescu-Zanetti, C.; Pope, M.; Li, J.; Nielson, L.; Ramirez-Alvarado, M.; Regan, L.; Fink, A. L.; Carter, S. A. *Biophys. J.* **2003**, *85*, 1135−1144.
(35) Hutter, J. L.; Bechhoefer, J. *Rev. Sci. Instrum.* **1993**, *64*, 1868−1873.
(36) Proksch, R.; Schäffer, T. E.; Cleveland, J. P.; Callahan, R. C.; Viani, M. B. *Nanotechnology* **2004**, *15*, 1344−1350.
(37) Burnham, N. A.; Colton, R. J. *J. Vac. Sci. Technol. A.* **1989**, *7*, 2906−2913.
(38) Bevington, P. R.; Robinson, D. K. *Data reduction and error analysis for the physical sciences*, 3rd ed.; McGraw-Hill: New York, 2003; pp 203−204.
(39) Dhaliwal, R. S.; Rau, I. S. *Int. J. Eng. Sci.* **1970**, *8*, 843−856.
(40) Rau, I. S.; Dhaliwal, R. S. *Int. J. Eng. Sci.* **1972**, *10*, 659−663.
(41) Morozov, V. N.; Morozova, T. Y. *J. Biomol. Struct. Dyn.* **1993**, *11*, 459−481.
(42) Alonso, J. L.; Goldmann, W. H. *Life Sci.* **2002**, *72*, 2553−2560.
(43) Dzwolak, W.; Ravindra, R.; Lendermann, J.; Winter, R. *Biochemistry* **2003**, *42*, 11347−11355.
(44) Perutz, M. F.; Finch, J. T.; Berriman, J.; Lesk, A. *Proc. Natl. Acad. Sci. U.S.A.* **2002**, *99*, 5591−5595.
(45) Nilsson, M. R.; Dobson, C. M. *Protein Sci.* **2003**, *12*, 2637−2641.
(46) Petkova, A. T.; Leapman, R. D.; Guo, Z.; Yau, W.; Mattson, M. P.; Tycko, R. *Science* **2005**, *307*, 262−265.

BM0600724